Journal of Hydroscience and Hydraulic Engineering
Vol. 10, No. 1, May, 1992, 11-25

VELOCITY DISTRIBUTION IN UNSTEADY OPEN-CHANNEL FLOW OVER GRAVEL BEDS

By

Haizhou Tu

Laboratoire de Recherches Hydrauliques
Ecole Polytechnique Fédérale, 1015 Lausanne, Switzerland
Presently: Dept. Civil Engineering, University of Tokyo, Tokyo 113, Japan

and

W. H. Graf

Laboratoire de Recherches Hydrauliques
Ecole Polytechnique Fédérale, 1015 Lausanne, Switzerland

SYNOPSIS

Velocity profiles during the passages of different hydrographs, simulated in a gravel-bed flume, have been measured, and are presented in this paper. It is seen that the log-law and the Coles law can also be used in unsteady open-channel flow. However, modifications should be made to take into consideration of the unsteadiness, represented herewith by the Clauser parameter. The Coles wake parameter indicates that the wake becomes more pronounced in the falling branch compared with the one in the rising branch. The present data are compared with those from other types of flow reported in the literature; it is shown that all the data, from steady or unsteady open-channel flow, over smooth or rough bed, follow the same tendency, despite considerable scatter.

INTRODUCTION

Unsteady flows are those whose properties depend also on time if referenced to an Eulerian frame. In natural rivers most of the flows are unsteady. However, unsteady phenomena are worth studying only if they depart substantially from quasi-steady state, or if treated with steady flow theory, significant errors would arise, such as flows in mountain streams characterized by steep slopes and gravel beds.

In the past, some experiments had been carried out to study unsteady flow in open channels, for example, at the University of Canterbury, New Zealand, and at the EPFL, Switzerland. The researches at these two institutions concern mainly with bedload transport in unsteady flow (1, 15, 8). Nakagawa and Tsujimoto (12) studied the time-lag phenomenon in unsteady flow over sand waves. Tsujimoto (17), using linear analysis to the data obtained by Suszka (16) and Phillips and Sutherland (15), discussed two mechanisms in unsteady sediment transport: the first due to the direct effect of flow unsteadiness, and the second brought by the relaxation process of the "fluvial system". Nouh (14) studied unsteady flow effect on the armoring layer in a straight open channel. Flume experiments were also conducted by Tubino (21) to investigate alternate-bars in unsteady flow. Recently, Tu and Graf (20) examined friction in unsteady flow over gravel beds.

Velocity distribution in unsteady flow has been studied in closed conduits (wind or water tunnels, pipes) by many researchers (4). However, there are few velocity-distribution data obtained from unsteady flow in open channels.

A more comprehensive review on the past unsteady-flow study as well as on gravel-bed flow study is provided in (19).

In the present laboratory study, different hydrographs (see Table 1) are simulated in a gravel-bed flume. Systematical measurements of the velocity profiles have been undertaken. The results are presented herein, and are subsequently analyzed.

EXPERIMENTS

The details of the unsteady flow experiments are given in [19], but are briefly described in the following.

In order to simulate meaningfully hydrographs in the laboratory, an examination of those in natural mountain rivers was undertaken. It was seen that a natural hydrograph is usually skewed, with the water depth increasing rapidly in the rising branch and subsequently decreasing slowly in the falling branch.

Keeping in mind the characteristics of natural hydrographs, different hydrographs - as an example see Fig.1 - were passed through a gravel-bed flume, which is 16.8m long, 0.6m wide and 0.8m high, with glass side walls and a smooth steel floor being covered with gravels. The parameters characterizing these hydrographs are given in Table 1, where the symbols appeared are defined in the end of this paper.

Three micropropellers, each with a diameter of 1.5cm, are used to measure the point velocities at three sections (Fig.2); the instantaneous water depth at each section was measured with a limnimeter. The lowest point for the velocity measurement is 0.75cm (i.e., half of the micropropeller's diameter) above the top surface of the grave bed, below which the reference-bed level is shifted at a distance of $0.25d_s$ (d_s is the gravel diameter) - see Fig.2 and Tu at el. (18). The micropropeller displace-ment was as follows: near the bottom the point velocities were measured every 2mm at 5 points; then measured every 5mm at another 5 points; from there on till the water surface the velocities were measured every 10mm. There were usually 23 to 26 measuring points in each station.

For unsteady flow, the velocity measurement at a given point in space should be carried out by repeating as many times as possible the same hydrograph. However, it was found that repeating more than five times hardly improve significantly the precision. Thus it was decided to repeat the measurements five times at each given point in space. The five values, obtained at the same point from the five measurements, and corresponding to each time instant, are then averaged. These averaged values are smoothed mathematically. They give the time-mean point velocity, though no information on the turbulence. The details of the data-treatment procedure are given in Tu (19).

The thus obtained velocity profiles, together with the water depth, D, allow to calculate the vertically-averaged velocity, V, as well as the flow discharge, Q. For hydrograph NS1(1), the time-records of V, Q and D, are given in Fig.1, where the friction velocity calculated from the St. Venant equation of motion, u_{*SV} (see 19), is also shown. The figure demonstrates what would be predicted with the kinematic-wave theory (5): at a given cross section in the channel, first the velocity, V, then the discharge, Q, and subsequently the water depth, D, come with their respective peaks.

Table 1 Data range of the hydrographs investigated

Hydro-graph No.	S_0	d_s (cm)	ΔT (s)	ΔT_r (s)	ΔT_f (s)	D(cm) (min.,max.)	V(cm/s) (min.,max.)	$F_r = V/\sqrt{gD}$ (min.,max.)
NS1(1)	0.002	1.35	110	36	61	(9.0, 21.2)	(40.8, 94.9)	(0.43, 0.66)
NS1(2)	0.002	1.35	110	38	59	(9.3, 22.0)	(36.3, 93.4)	(0.38, 0.64)
NS1(3)	0.002	1.35	110	38	59	(9.9, 22.5)	(39.7, 97.7)	(0.40, 0.66)
NS2(1)	0.002	1.35	220	76	129	(6.6, 21.6)	(30.7, 96.1)	(0.38, 0.67)
NS2(2)	0.002	1.35	220	68	135	(7.0, 22.5)	(28.4, 95.7)	(0.34, 0.65)
NS2(3)	0.002	1.35	220	80	129	(7.2, 23.2)	(29.1, 95.9)	(0.34, 0.64)
NS3(1)	0.002	2.30	110	46	53	(14.2, 24.7)	(68.3, 122.9)	(0.58, 0.81)
NS3(2)	0.002	2.30	110	46	55	(15.4, 27.0)	(61.8, 120.0)	(0.50, 0.75)
NS3(3)	0.002	2.30	110	46	55	(15.7, 27.0)	(60.5, 121.5)	(0.48, 0.76)
NS4(1)	0.002	2.30	220	72	139	(11.5, 24.9)	(58.7, 123.7)	(0.55, 0.81)
NS4(3)	0.002	2.30	220	74	137	(12.9, 27.2)	(49.1, 115.6)	(0.44, 0.73)
NS5(1)	0.005	2.30	110	52	51	(13.0, 23.6)	(76.0, 130.9)	(0.68, 0.87)
NS5(3)	0.005	2.30	110	48	55	(13.8, 25.5)	(68.4, 129.4)	(0.59, 0.83)

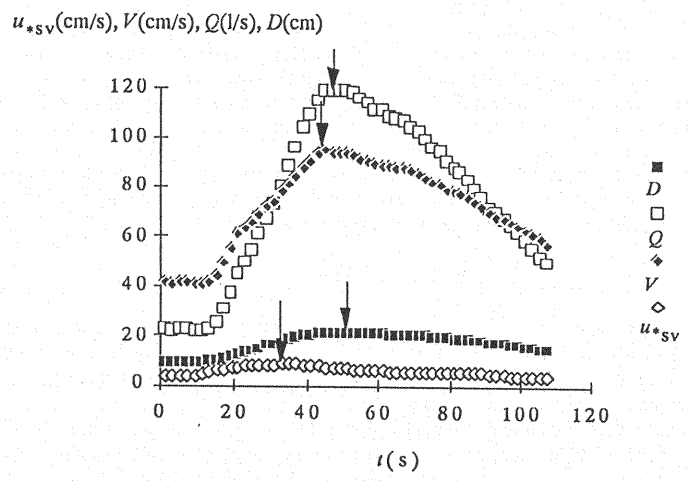

Fig.1 Time-records of u_{*SV}, V, Q and D; in hydrograph NS1(1)

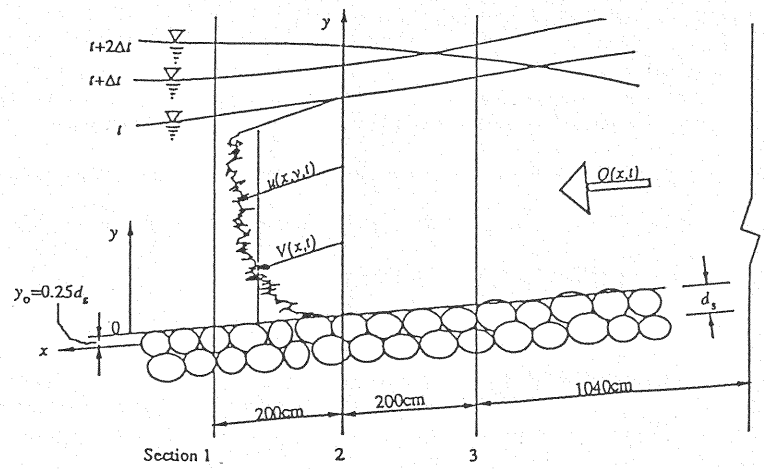

Fig.2 Experimental setup (the installation sketch)

VELOCITY PROFILES

In the following, if not specified otherwise, hydrograph NS1(1) - see Table 1 - will be used as an illustrative example for the presentation of velocity profiles.

Point-velocity variation with time and water height

Figure 3 gives the time variations of point velocities, $u(x,y,t)$, at different levels within the entire water depth (note that for each hydrograph the measurements were performed at 23 to 26 different levels). It can be observed that throughout the water column, the point velocities near the water surface arrive at their maximum values earlier than those near the bottom. This is due to the fact that the relative importance of inertia over viscosity forces gets greater as one moves away from the bed. With the point velocities as shown in Fig.3, one can now obtain the velocity profile at any time instant.

Evolution of the velocity profiles

The evolution of the vertical velocity profiles during the passage of hydrograph NS1(1), for several different time instants, is shown in Fig.4(1). The velocity distributions at t=21s, 41s, 61s, 81s and 101s, being each 20 seconds apart, are selected here for presentation. The corresponding hydraulic parameters are summarized in a table (see also Table 2). During the passage of the hydrograph, the velocity profiles get less full in the rising branch, subsequently getting fuller in the falling branch and tend to return towards the original shape. From the table in Fig.4(1) one can see the evolution of the discharge, Q, the water depth, D, the vertically-averaged velocity, V, as well as the friction velocity calculated from the St. Venant equation of motion, u_{*SV} (20), during the passage of the hydrograph (see also Fig.1).

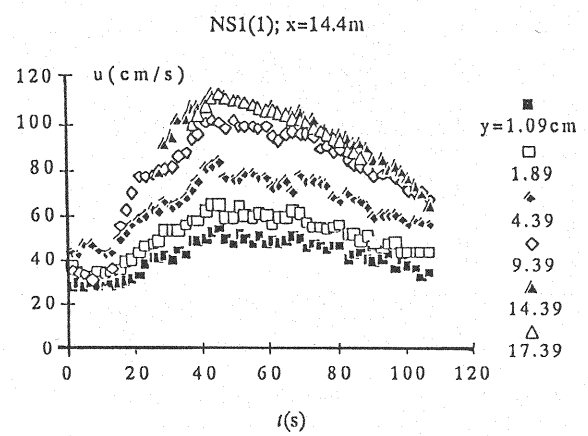

Fig.3 Point velocity, $u(x,y,t)$, variations with time, t, and water height, y

Velocity profiles in the rising and falling branch; for equal water depth

The velocity profiles in the rising and falling branch, for equal water depth, D, are shown in Fig.4(2). It is seen that:

1) at the same water height, y, here given as y/D, the point velocity, u, in the rising branch is generally larger than the one in the falling branch. The opposite is sometimes observed, called the "crossing phenomenon", near the bottom (Fig.5);

2) this difference of the point velocities, u, between the rising and the falling branch gets larger on approaching the water surface;

3) this difference of the point velocities, u, with the increase of the water depth, D, in approaching the peak of the wave, becomes smaller.

Similar observations are reported by Suszka (16) and Grishanin (9).

Velocity profiles in the rising and falling branch; for equal vertically-averaged velocity

The velocity profiles in the rising and falling branch, for equal vertically-averaged velocity, V, are shown in Fig.6, with the corresponding hydraulic parameters listed in a table. It is observed that, except for the part near the water surface, the two velocity profiles almost converge into the same curve.

ANALYSIS

In the above, the evolution of the velocity profiles during the passage of a hydrograph, as well as the velocity profiles in the rising and falling branch for equal water depth, D, or for equal vertically-averaged velocity, V, are presented. They shall now be analyzed.

The velocity distribution in steady flow over gravel beds can be described (18): either by the log-law, being valid in the inner region of the boundary layer:

$$\frac{u}{u_*} = \frac{1}{\kappa} \ln \frac{y+y_0}{d_s} + Br \qquad (1)$$

or by the Coles law, being valid in both the inner and outer region, thus throughout the entire boundary layer (18):

$$\frac{u}{u_*} = \frac{1}{\kappa} \ln \frac{y+y_0}{d_s} + Br + \frac{2\Pi}{\kappa} \sin^2\left(\frac{\pi}{2} \frac{y+y_0}{D'+y_0}\right) \qquad (2)$$

where u = the point velocity; y = water height above the top surface of the gravel bed; y_0 = the reference-level adjustment, taken as $y_0 = 0.25 d_s$ (see Fig.2, and Tu et al. (18)); d_s = the gravel diameter; D' = the water height where the maximum point velocity in a velocity profile, u_{max}, is measured; κ = the Karman constant; Br = a numerical constant of integration; Π = the Coles parameter expressing the wake strength; and $u_* = u_{*sv}$, the friction velocity determined with the St. Venant equation of motion for unsteady flow, such as (20):

$$u_{*sv} = \sqrt{g D\left(S_o - \frac{\partial D}{\partial x} - \frac{V}{g}\frac{\partial V}{\partial x} - \frac{1}{g}\frac{\partial V}{\partial t}\right)}$$

in which: t = is the time variable; D = the water depth; V = the vertically-averaged velocity; x = the longitudinal coordinate; and S_o = the bottom slope.

The question here is whether or not Eqs.1 and 2 still hold in unsteady flow; this will be seen in the following.

The velocity profiles in Fig.4 are replotted in dimensionless form as u/u_{*sv} versus $(y+y_0)/d_s$ in Fig.7. It is seen that the log-law and the Coles law remain valid. Like in steady flow, the Br-values and the Π-values can be determined for each of the velocity profiles, as indicated in the insert of Fig.7. In all, 273 velocity profiles have been analyzed (19). In this paper, if not specified otherwise, only 65 velocity profiles - covering the evolution of the entire hydrographs (Fig.7(1)) - will be presented. The obtained Br-values and Π-values, together with other hydraulic parameters, are listed in Table 2, and discussed in the following paragraphs. In Table 2 the terms, $\frac{\partial V}{\partial t}$ and $V\frac{\partial V}{\partial x} = -\frac{V}{C}\frac{\partial V}{\partial t}$, are calculated from the time-records of the vertically-averaged velocity, $V(x, t)$. Note that, using the kinematic-wave theory, the spatial acceleration $\frac{\partial V}{\partial x}$, can be expressed by $-\frac{1}{C}\frac{\partial V}{\partial t}$, where C is the the wave velocity, being given as $C = V + D\frac{\partial V}{\partial t}/\frac{\partial D}{\partial t}$ (20).

1) the evolution of the velocity profiles

t	D	V	Q	u_{*sv}
21	12.2	60.6	44.5	7.3
41	20.1	90.5	109.3	8.0
61	20.7	88.9	110.7	6.0
81	18.7	78.2	87.9	5.7
101	15.5	62.8	58.6	4.0

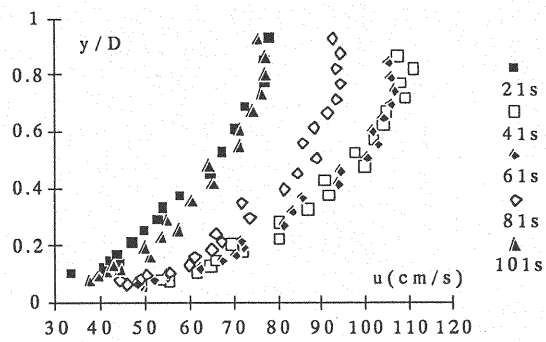

2) the velocity profiles in the rising and falling branch, for equal water depth

	rising branch				falling branch			
D(cm)	t(s)	V(cm/s)	Q(l/s)	u_{*sv} (cm/s)	t(s)	V(cm/s)	Q(l/s)	u_{*sv} (cm/s)
14.6	27.0	69.1	60.7	8.0	105.0	59.1	52.3	3.8
16.3	31.0	74.4	72.9	8.3	95.0	67.9	67.4	4.6
18.9	37.0	84.3	95.9	8.4	79.0	79.2	90.0	5.8
20.5	43.0	93.2	114.9	7.7	59.0	89.2	111.0	6.1

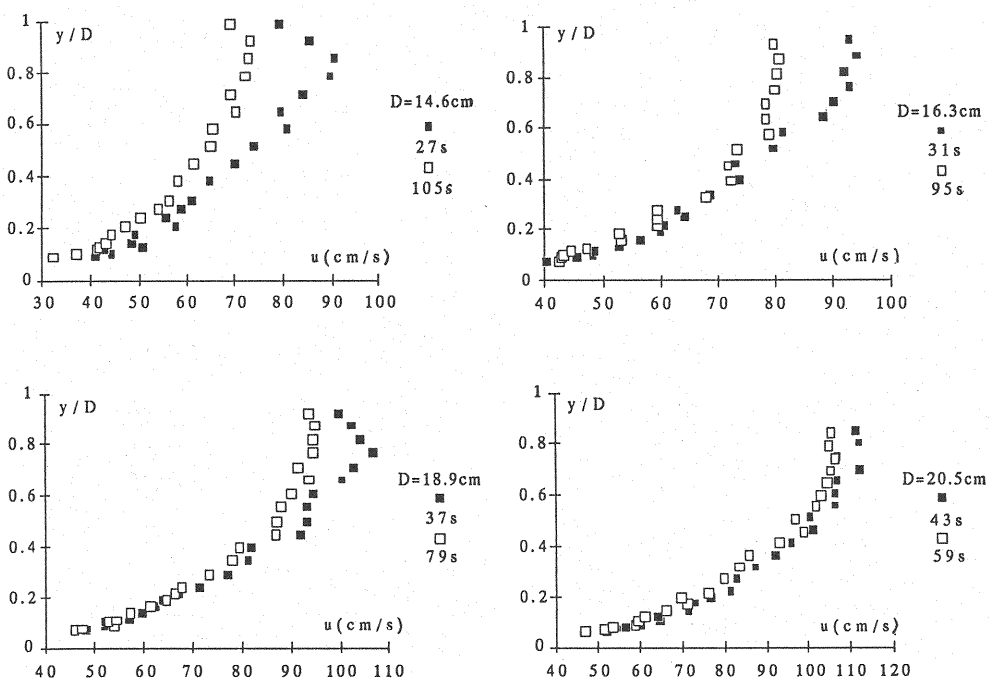

Fig.4 Velocity profiles: 1) the evolution; 2) in the rising and falling branch, for equal water depth, D; in hydrograph NS1(1)

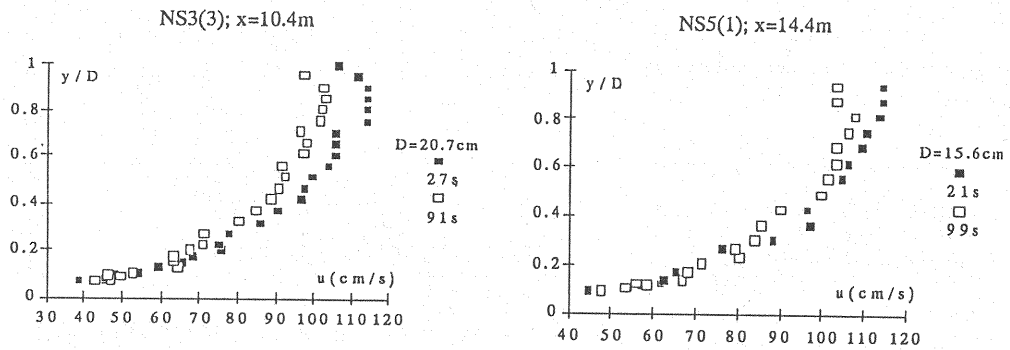

Fig.5 the "Crossing phenomenon"

V	rising branch				falling branch			
	t	D	Q	u_{*sv}	t	D	Q	u_{*sv}
(cm/s)	(s)	(cm)	(l/s)	(cm/s)	(s)	(cm)	(l/s)	(cm/s)
55.1	19.0	11.2	37.2	7.0	107.0	14.3	49.2	3.6
66.0	25.0	13.7	54.4	7.8	97.0	16.2	64.0	4.3
78.5	33.0	17.1	80.7	8.4	81.0	18.7	87.9	5.7
87.8	39.0	19.7	103.9	8.3	67.0	20.1	106.3	5.8

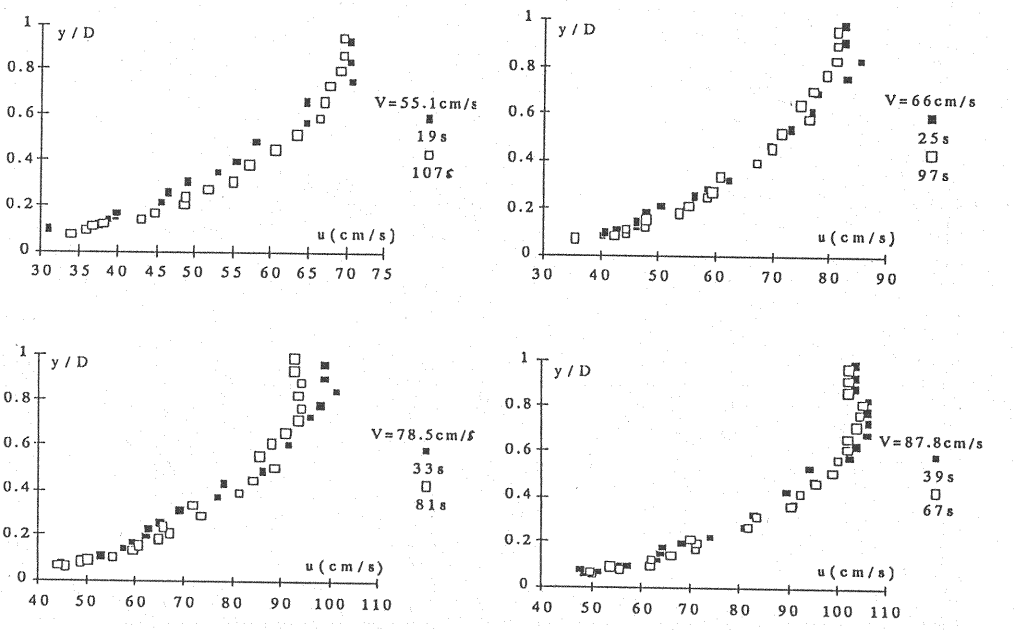

Fig.6 Velocity profiles in the rising and falling branch,
for equal vertically-averaged velocity, V;
in hydrograph NS1(1)

1) the evolution of the velocity profiles

t	D	V	u_{*sv}	Br	Π
21	12.2	60.6	7.3	4.9	0.18
41	20.1	90.5	8.0	6.8	0.25
61	20.7	88.9	6.0	9.2	0.55
81	18.7	78.2	5.7	9.2	0.31
101	15.5	62.8	4.0	10.0	0.72

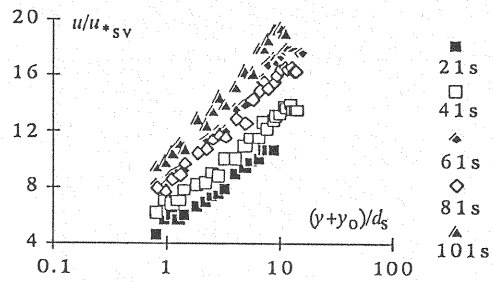

2) the velocity profiles in the rising and falling branch, for equal water depth

	rising branch					falling branch				
D (cm)	t (s)	V (cm/s)	u_{*sv} (cm/s)	Br	Π	t (s)	V (cm/s)	u_{*sv} (cm/s)	Br	Π
14.6	27.0	69.1	8.0	4.5	0.30	105.0	59.1	3.8	10.0	0.72
16.3	31.0	74.4	8.3	5.0	0.00	95.0	67.9	4.6	9.4	0.41
18.9	37.0	84.3	8.4	5.3	0.30	79.0	79.2	5.8	8.5	0.44
20.5	43.0	93.2	7.7	7.1	0.24	59.0	89.2	6.1	9.1	0.47

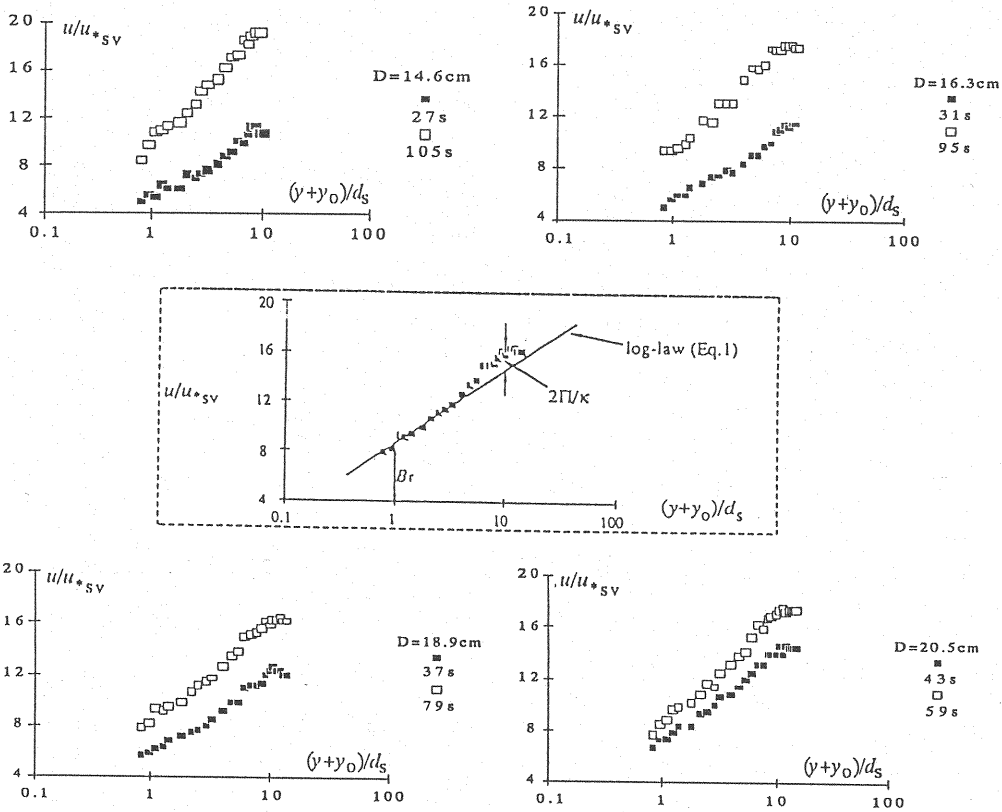

Fig.7 Dimensionless velocity profiles, u/u_{*sv} versus $(y+y_0)/d_s$;
in hydrograph NS1(1)

Table 2 Hydraulic parameters and Br and Π-values in the hydrographs investigated

t(s)	D (cm)	V (cm/s)	$\frac{V^2}{gD}$	$\frac{d_s}{D+y_o}$	$\frac{\partial V}{\partial t}$ (cm/s.s)	C (cm/s)	$V\frac{\partial V}{\partial x}$ (cm/s.s)	β	u_{*sv} (cm/s)	Br	Π
NS1(1)											
21	12.2	60.6	0.31	0.108	1.932	118.5	-0.988	-0.17	7.3	4.9	0.18
41	20.1	90.5	0.42	0.066	0.764	154.0	-0.449	-0.05	8.0	6.8	0.25
61	20.7	88.9	0.39	0.064	-0.475	193.5	0.218	0.05	6.0	9.2	0.55
81	18.7	78.2	0.33	0.071	-0.686	188.8	0.284	0.08	5.7	9.2	0.31
101	15.5	62.8	0.26	0.085	-0.820	132.7	0.388	0.10	4.0	10.0	0.72
NS1(2)											
21	13.0	59.8	0.28	0.101	2.098	125.2	-1.002	-0.22	7.3	3.8	0.31
41	20.7	90.7	0.41	0.064	0.632	148.6	-0.386	-0.04	8.1	5.0	0.41
61	21.3	86.7	0.36	0.062	-0.607	246.3	0.214	0.08	6.6	5.8	0.87
81	19.2	71.5	0.27	0.069	-0.858	194.4	0.316	0.13	5.9	5.8	0.57
101	15.9	55.2	0.20	0.083	-0.840	128.6	0.361	0.15	4.1	6.1	0.93
NS1(3)											
21	13.9	67.1	0.33	0.095	2.045	132.3	-1.037	-0.18	7.6	5.1	0.00
41	21.6	96.4	0.44	0.062	0.517	150.9	-0.330	-0.03	8.2	6.7	0.10
61	22.0	87.6	0.36	0.060	-0.693	264.9	0.229	0.09	6.8	8.2	0.13
81	19.7	71.7	0.27	0.067	-0.941	206.0	0.328	0.15	6.1	7.3	0.10
101	16.4	54.1	0.18	0.081	-0.195	119.5	0.088	0.04	3.6	9.0	0.67
NS2(1)											
41	14.6	65.2	0.30	0.090	1.087	123.8	-0.572	-0.10	7.2	4.9	0.26
81	21.4	95.8	0.44	0.062	0.162	161.2	-0.096	-0.01	6.9	7.4	0.31
121	20.1	89.2	0.40	0.066	-0.296	180.7	0.146	0.03	5.9	8.5	0.72
161	17.5	75.5	0.33	0.076	-0.413	163.6	0.191	0.04	5.4	8.5	0.41
201	13.6	54.9	0.23	0.097	-0.509	117.8	0.237	0.07	4.2	8.5	0.41
NS2(2)											
41	15.4	64.0	0.27	0.086	1.077	125.9	-0.547	-0.12	7.4	4.5	0.15
81	22.5	95.6	0.41	0.059	0.129	150.4	-0.082	-0.01	7.1	7.4	0.51
121	21.0	85.2	0.35	0.063	-0.361	196.0	0.157	0.04	6.2	7.4	0.51
161	18.2	68.1	0.26	0.073	-0.455	172.9	0.179	0.07	5.7	6.7	0.31
201	14.3	49.9	0.18	0.092	-0.423	103.0	0.205	0.07	4.0	7.4	0.51
NS2(3)											
41	15.9	66.4	0.28	0.083	0.982	123.8	-0.527	-0.10	7.6	4.6	0.10
81	23.1	95.9	0.41	0.058	0.088	136.6	-0.062	0.00	7.3	7.7	0.26
121	21.6	83.3	0.33	0.062	-0.365	189.8	0.160	0.04	6.2	7.7	0.31
161	18.5	66.5	0.24	0.072	-0.492	180.3	0.181	0.08	5.8	6.7	0.26
201	14.6	48.5	0.16	0.090	-0.371	96.0	0.187	0.07	3.8	7.7	0.55
NS3(1)											
21	16.9	83.3	0.42	0.132	1.642	193.4	-0.707	-0.11	6.2	9.5	0.53
41	21.7	115.4	0.63	0.103	1.119	217.9	-0.593	-0.05	7.4	10.2	0.69
61	24.3	118.3	0.59	0.092	-0.622	398.2	0.185	0.04	7.4	10.2	0.61
81	21.2	101.8	0.50	0.106	-0.980	201.7	0.495	0.05	5.5	12.0	0.99
101	16.4	78.9	0.39	0.135	-1.070	156.5	0.539	0.07	4.2	14.2	0.84
NS3(2)											
21	18.4	78.7	0.34	0.121	1.997	217.4	-0.723	-0.20	5.9	8.4	0.77
41	24.0	113.0	0.54	0.094	0.822	186.3	-0.499	-0.04	8.6	8.5	0.46
61	26.4	112.8	0.49	0.085	-0.652	304.1	0.242	0.05	7.4	9.1	0.85
81	23.0	96.7	0.41	0.098	-1.028	202.3	0.491	0.08	5.7	11.0	0.92
101	17.9	72.4	0.30	0.124	-1.173	164.1	0.518	0.12	4.7	10.2	1.00
NS3(3)											
21	19.0	80.6	0.35	0.117	2.198	239.4	-0.740	-0.23	5.5	10.2	0.32
41	24.2	115.4	0.56	0.093	0.786	192.4	-0.471	-0.03	8.4	9.1	0.38
61	26.5	113.0	0.49	0.085	-0.793	451.9	0.198	0.07	8.0	9.1	0.46
81	23.2	95.1	0.40	0.097	-1.099	197.1	0.530	0.08	5.5	12.0	0.69
101	18.0	66.5	0.25	0.124	-1.324	180.5	0.488	0.18	5.5	8.5	0.61
NS4(1)											
41	17.4	87.3	0.45	0.128	1.277	186.9	-0.596	-0.08	6.5	9.5	0.62
81	24.9	123.7	0.63	0.090	0.110	166.5	-0.082	0.00	7.6	11.3	0.77
121	22.6	107.0	0.52	0.099	-0.494	202.4	0.261	0.03	6.1	12.5	0.92
161	17.7	88.9	0.46	0.126	-0.524	188.6	0.247	0.03	5.6	11.3	0.85
201	13.9	66.1	0.32	0.159	-0.522	128.7	0.268	0.04	4.3	12.5	0.65
NS4(3)											
41.0	19.2	79.0	0.33	0.116	1.307	182.7	-0.565	-0.12	7.0	7.1	0.57
81.0	27.0	112.5	0.48	0.083	-0.001	112.1	0.001	0.00	8.2	8.5	0.57
121.0	24.5	96.3	0.39	0.092	-0.492	193.5	0.245	0.04	6.2	12.1	0.74
161.0	19.5	74.2	0.29	0.115	-0.577	178.4	0.240	0.06	5.8	8.5	0.63
201.0	15.0	52.8	0.19	0.148	-0.421	105.9	0.210	0.05	4.0	9.6	0.66
NS5(1)											
21	15.6	90.9	0.54	0.142	1.687	180.1	-0.851	-0.08	9.4	6.8	0.15
41	21.0	122.9	0.73	0.107	1.041	221.4	-0.578	-0.04	10.7	8.4	0.20
61	23.3	125.6	0.69	0.096	-0.544	348.0	0.196	0.03	10.9	7.8	0.18
81	19.9	109.6	0.62	0.112	-1.101	218.6	0.552	0.05	9.5	7.8	0.30
101	15.2	85.4	0.49	0.146	-1.144	157.9	0.619	0.05	7.7	8.4	0.20
NS5(3)											
21	17.0	87.8	0.46	0.131	1.881	196.6	-0.840	-0.12	9.5	6.3	0.10
41	22.4	120.9	0.67	0.100	0.931	204.3	-0.551	-0.03	10.3	7.9	0.25
61	24.4	119.1	0.59	0.092	-0.755	333.3	0.270	0.05	11.2	7.0	0.17
81	21.0	99.6	0.48	0.107	-1.456	226.5	0.640	0.09	9.9	6.8	0.18
101	15.8	69.4	0.31	0.140	-1.064	151.4	0.488	0.09	8.1	6.0	0.16

Clauser's parameter

Unsteady flow is accelerative or decelerative, having a longitudinal pressure gradient, $dp_e/dx < 0$ or $dp_e/dx > 0$. A dimensionless pressure gradient, derived by considering the Karman's integral equation (7), is given as:

$$\beta = \frac{\delta^*}{\tau_0}\frac{dp_e}{dx} \tag{3}$$

being $\beta < 0$ and $\beta > 0$ for accelerating and decelerating flow, respectively. This parameter, β, is also known as the Clauser equilibrium parameter (22), where δ^*, τ_0 and p_e are the displacement thickness, the bottom shear stress and the freestream pressure, respectively.

From the reasoning of boundary-layer hydrodynamics, the equation of motion for an incompressible fluid (along a streamline), at the outer edge of the boundary layer is written as:

$$\frac{du_{max}}{dt} = \frac{\partial u_{max}}{\partial t} + u_{max}\frac{\partial u_{max}}{\partial x} = -\frac{1}{\rho}\frac{dp_e}{dx} \tag{4}$$

where u_{max} is the point velocity at the edge of the boundary layer, and the free-stream pressure, p_e, is assumed to penetrate the entire boundary layer unchanged.

Thus the Clauser parameter, β, can also be written as:

$$\beta = \frac{\delta^*}{\tau_0}\frac{dp_e}{dx} = -\frac{\rho\delta^*}{\tau_0}\left(\frac{\partial u_{max}}{\partial t} + u_{max}\frac{\partial u_{max}}{\partial x}\right) \tag{5}$$

In order to compare the present unsteady-flow data with those from other types of flow reported in the literature, it is necessary to calculate the β-values for the present data. This is done as follows.

The Clauser parameter, given with Eq.5, can be written as:

$$\beta = \frac{\delta^*}{\tau_0}\frac{dp_e}{dx} = -\frac{\delta^*}{u_*^2}\frac{du_{max}}{dt} \tag{6}$$

To calculate the β-value, one needs to know: the displacement thickness, δ^*, the friction velocity, u_*, and the total acceleration, du_{max}/dt. These terms can be determined using the following two assumptions, both based on the fact that the velocity distribution in the present open-channel flow study follows the log-law (Fig.7):

(*i*) the velocity profile over the entire water depth can be expressed in form of a power law:

$$\frac{u}{u_{max}} = \left(\frac{y}{D}\right)^{1/m} \tag{7}$$

where m is an exponent, which is given for a plane-bed river as (11):

$$\frac{1}{m} = \frac{1}{4.7}\left(\frac{d_s}{D}\right)^{0.06} \tag{8}$$

(*ii*) the velocity gradient near the bed is given by $du/dy = u_*/(\kappa y)$; thus the friction velocity can be expressed as:

$$u_* = \kappa y \left.\frac{du}{dy}\right|_{y=d_s} \tag{9}$$

Using Eq.7, the flow discharge per unit width is given by:

$$q = VD = \int_0^D u\,dy = \frac{m}{1+m}Du_{max}$$

Subsequently, the displacement thickness, δ^*, and the maximum velocity, u_{max}, are derived, respectively, as:

$$\delta^* = \int_0^D (1 - \frac{u}{u_{max}})\,dy = D\,(1 - \frac{V}{u_{max}}) = \frac{1}{1+m} D\,; \quad \text{and} \quad \frac{u_{max}}{V} = 1 + \frac{1}{m} \tag{10}$$

With Eqs.7, 9 and 10 an expression for the friction velocity is written as:

$$u_* = \kappa y\, u_{max} \frac{1}{m} (\frac{y}{D})^{1/m-1} \frac{1}{D} \Big|_{y=d_s} = \frac{\kappa(1+m)}{m^2} V (\frac{d_s}{D})^{1/m} \tag{11}$$

The expressions of δ^* and u_{max} in Eq.10 and of u_* in Eq.11, are used to rewrite the Clauser parameter, β, defined with Eq.6 for unsteady open-channel flow, as follows:

$$\beta = \frac{m^3}{[\kappa(1+m)(\frac{d_s}{D})^{1/m}]^2} (-\frac{D}{V^2} \frac{dV}{dt}) \tag{12}$$

The Clauser parameter, β, evaluated with Eq.12 - in using Eq.8 - is given in Table 2.

The calculation of the Clauser parameter, β, using Eq.12, makes it possible (as will be discussed in the following) to compare the present data set with those from other types of flow. It is noted, however, that this calculation is approximative. The two main reasons are: *firstly*, Eq.4 can only be used when a boundary-layer flow exists in the open channel, which can not be taken as guaranteed, since a boundary-layer flow is different from an open-channel flow; *secondly*, Eq.8 implies that for an equal water depth, the velocity profiles in both the rising and falling branch have the same m-value, or independent of the flow unsteadiness. This is also questionable, although a similar tendency was always observed by plotting (not shown here) the Π-values given in Tu (19) versus the β-values calculated from different combinations of the maximum and minimum m-values and d_s/D-values.

Br-values

In steady flow, the Br-value varies with the relative roughness (18), $d_s/(D+y_0)$. It is taken as being a constant of Br = 8.5 for small relative roughness, say $d_s/(D+y_0) < 0.05$ (6). In unsteady flow, in addition to the relative roughness, the flow unsteadiness may also influence the Br-value. The β-value determined with Eq.12, which includes the term of unsteadiness, dV/dt, will be considered as an unsteadiness parameter.

Br-values versus the relative roughness, $d_s/(D+y_0)$

In Fig.8 are plotted the Br-values (from Table 2) versus the relative roughness, $d_s/(D+y_0)$. It shows that, while the Br-values vary in the range of $3.8 < Br < 14.5$ with the relative roughness in the range of $0.058 < d_s/(D+y_0) < 0.16$, the Br-value may be represented by a constant, being $Br \approx 8.5$. Note that the data from hydrograph NS1 [including NS1(1), NS1(2), NS1(3)] are drawn with a different symbol from the other unsteady flow data, so that the Br-value variations in a particular hydrograph can be observed.

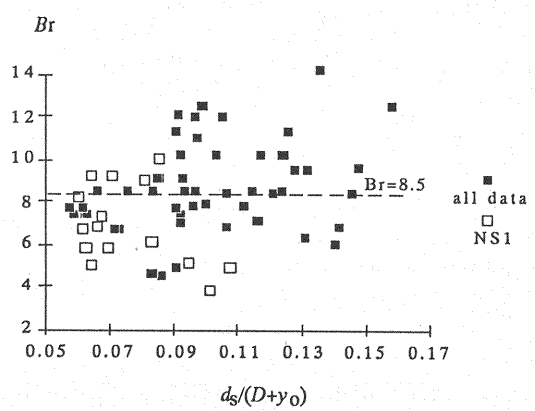

Fig.8 Br-value versus the relative roughness, $d_s/(D+y_0)$

Br-values versus the Clauser parameter, β

A simple regression analysis for all the data (273 velocity profiles, see (19)) renders for the *Br*-values an empirical relation, such as:

$$Br = 8.1\,\beta + 8.1 \qquad (13)$$

This relation is shown by the broken line in Fig.9, together with the data from the 65 velocity profiles given in Table 2. Despite the scatter, a certain tendency is evident: for accelerating flow (rising branch), the *Br*-values are lower than the ones for decelerating flow (falling branch). For hydrograph NS1(1) this can also be observed in Fig.7.

Br-value variations with time, t

The *Br*-values variations with time, for hydrographs NS1(1), NS1(2) and NS1(3), are shown in Fig.10. It is seen that the *Br*-values show an increasing tendency during the passage of the hydrographs; being lower in the rising branch (accelerating flow) and usually higher in the falling branch (decelerating flow) of each hydrograph.

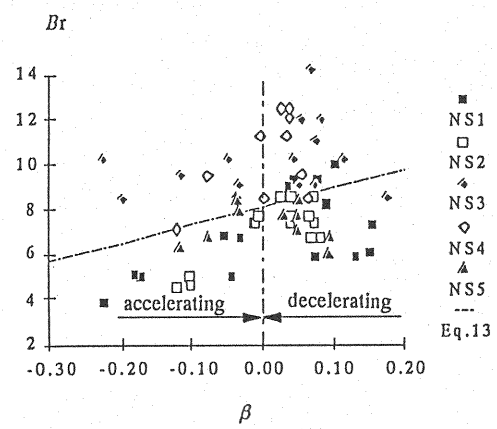

Fig.9 *Br*-value versus the Clauser parameter, β

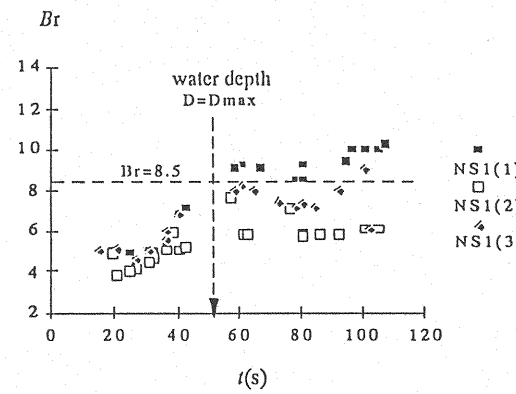

Fig.10 *Br*-value variations during the passage of different hydrographs

Π-values

Π-values versus the Clauser parameter, β: in boundary-layer flow

It is common in fluid mechanics to correlate the wake-strength parameter, *Π*, of Eq.2, with the Clauser equilibrium parameter, *β*. An empirical expression, being valid for equilibrium and "even for non-equilibrium" boundary-layer flows, such as:

$$\Pi \approx 0.8(\beta+0.5)^{0.75} \qquad \text{if } \beta > -0.5 \qquad (14)$$

was proposed by White (22).

Graf and Altinakar (7) presented an analysis of the *Π*-value, based on the existing data in the literature. For flow without pressure gradient, $dp_e/dx = 0$, obviously $\beta = 0$, and the *Π*-values become $\Pi \cong 0.55$, which corroborates with boundary-layer data by Klebanoff. For positive pressure gradient, $dp_e/dx > 0$, one has $\beta > 0$ and the *Π*-values become $\Pi > 0.55$, which corroborates with boundary-layer data by Clauser. For negative pressure gradient, $dp_e/dx < 0$, one has $\beta < 0$ and the *Π*-values become $\Pi < 0.55$, which corroborates with boundary-layer data by Herring et al. and with pipe-flow data by Nikuradse.

Π-values versus the Clauser parameter, β: in unsteady open-channel flow

A simple regression analysis for all the data (273 velocity profiles, see (19)) renders for the *Π*-values an empirical relation, such as:

$$\Pi = 1.02\,\beta + 0.46 \qquad (15)$$

This relation is shown by the solid line in Fig.11, together with the data from Table 2. The empirical relation from boundary-layer flow (Eq.14) is represented with the broken line. While the scatter is considerable, it is seen that the present unsteady open-channel flow data follow a similar trend as do the data from boundary-layer flow. The scattering in Fig.11 is

explained (19) by the fact that a small error in measuring the maximum velocity, u_{max}, the water depth, D (or the boundary layer thickness) and the friction velocity, u_*, can produce a remarkable error in the Π-value.

Π-values versus the Clauser parameter, β: in different types of open-channel flow

There are a few studies on open-channel flow available in the literature with which the present data set should be compared; this is shown in Fig.12. Data from uniform flow over smooth bed, being of slightly accelerating type, are reported by Nezu and Rodi (13) and by Cardoso et al. (2). Data from steady flow over smooth and rough beds, of gradually accelerating and decelerating types, are reported by Cardoso et al. (3) and Kironoto and Graf (10), respectively. For the sake of comparison, Eq.15 being a fit to the present data and Eq.14 being a fit to the boundary-layer data, are also plotted. Figure 12 shows that all the data, from steady or unsteady open-channel flow, over smooth or rough bed, follow the same tendency, despite considerable scatter.

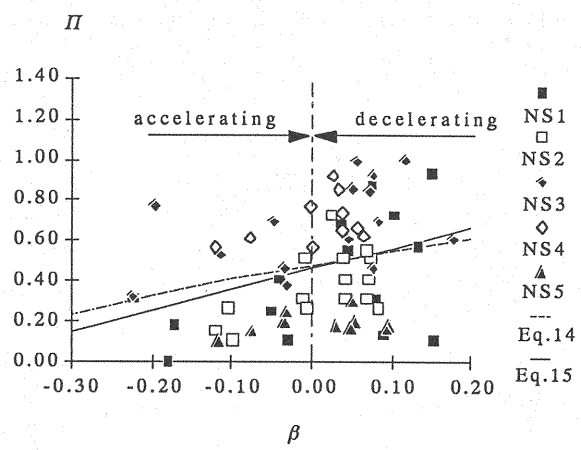

Fig.11 Π-value versus the Clauser parameter, β

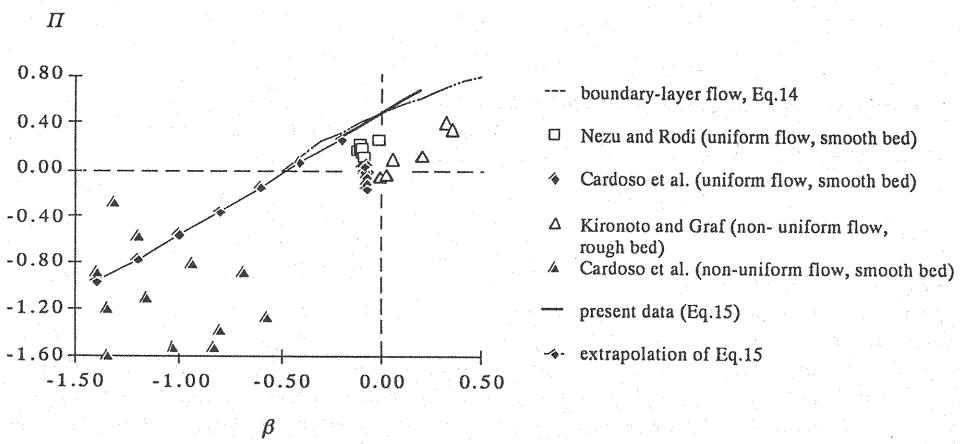

Fig.12 Π-value versus the Clauser parameter, β; for different types of open-channel flow

Π-value variations with time, t

The Π-value variations with time, for hydrographs NS1(1), NS1(2) and NS1(3), are shown in Fig.13. It is seen that the Π-values have a tendency to increase during the passage of the hydrographs. The wake becomes more pronounced in the falling branch (decelerating flow) compared with the one in the rising branch (accelerating flow). For hydrograph NS1(1), this can also be observed in Fig.7.

VERTICALLY-AVERAGED VELOCITY

For steady flow over gravel beds, Tu et al. (18) have shown that the vertically-averaged velocity, V, can be measured directly at a point where the relative water depth is $y/D \approx 0.4$. Whether this remains true in unsteady flow is to be seen in the following. Here we continue to designate the aforementioned relative water depth as $(y/D)_{av}$.

In Fig.14 is plotted the time variation of $(y/D)_{av}$ for hydrograph NS2(1). The time variation of $(y/D)_{av}$ for all the other hydrographs are given in Tu (19). It is seen from Fig.14 that $(y/D)_{av}$ can not be assumed as a constant of 0.4 during a hydrograph. Being slightly smaller than 0.4 during most part of the hydrograph, it decreases in the rising branch and then increases to return to about 0.4 in the falling branch.

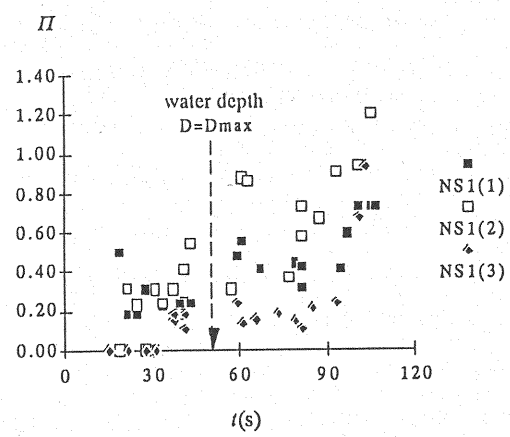

Fig.13 Π-values variation with time, t

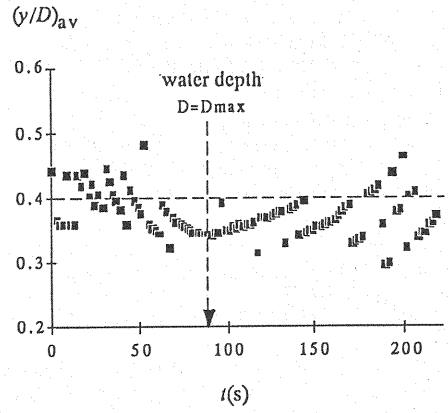

Fig.14 Time variation of the relative water depth, $(y/D)_{av}$, in hydrograph NS2(1)

CONCLUSIONS

Velocity profiles in unsteady flow over gravel beds have been measured, and are presented and analyzed in this paper. The major results can be summarized in the following.

1) The point velocities near the water surface arrive at their maximum values earlier than those near the bottom (Fig.3).

2) For an equal water depth, the point velocity in the rising branch is generally larger than the one in the falling branch (Fig.4(2)); however, the inverse may occur (Fig.5). For an equal vertically-averaged velocity, the velocity profiles fall almost one on the other, except near the water surface where the point velocities in the rising branch are usually larger than the ones in the falling branch (Fig.6).

3) The log-law (Eq.1) and the Coles law (Eq.2) can also be used in unsteady flow (Fig.7).

4) The Clauser parameter, β, has been calculated (Eq.12) for unsteady open-channel flow using some reasonable assumptions; for the hydrographs investigated a variation in the range of $-0.23 < \beta < 0.18$ was found (Fig.11).

5) The Br-values, varying in the range of $3.8 < Br < 14.5$ with the relative roughness in the range of $0.058 < d_s/(D+y_o) < 0.16$, may be represented by an average value of $Br \approx 8.5$ (Fig.8). For accelerating flow (in the rising branch and $\beta < 0$), the Br-values are lower than the ones for decelerating flow (in the falling branch and $\beta > 0$) (Figs.9 and 10).

6) The Π-values versus the Clauser parameter, for all the hydrographs are shown in Fig.11. The present data are compared with boundary-layer flow data as well as other open-channel flow data in Fig.12, which shows that all the data follow the same tendency, despite considerable scattering. It is seen from the time variation of the Π-values (Fig.13) that the wake becomes more pronounced in the falling branch (decelerating flow) compared with the one in the rising branch (accelerating flow).

7) The relative water depth, $(y/D)_{av}$, where the point velocity equals the vertically-averaged velocity, can not be assumed as a constant of 0.4 during a hydrograph (Fig.14).

8) The present set of experiments and the conclusions drawn herewith should be regarded as being indicative; only larger variations of the parameters - in future studies to be done - will or will not be confirmative.

REFERENCES

1. Bell, R. G. (1980), Non-Equilibrium Bedload Transport by Steady and Non-Steady Flows, Report 80/23, Dept. Civil Engineering, Univ. Canterbury, New Zealand.

2. Cardoso, A. H., W. H. Graf and G. Gust (1989), Uniform Flow in Smooth Open Channel, J. Hydr. Res., Vol.27, No.4.
3. Cardoso, A. H., W. H. Graf and G. Gust (1991), Steady Gradually Accelerating Flow in A Smooth Open Channel, J. Hydr. Res., Vol.29, No.3.
4. Carr, L.W., (1981) A Review of Unsteady Turbulent Boundary-Layer Experiments, in Unsteady Turbulent Shear Flows, IUTAM Symposium, Toulouse, France, Michel.R. et al. eds.
5. Forchheimer, p. (1930), Hydraulik, Teubner Verlagsgesellschaft, Leipzig and Berlin.
6. Graf, W.H. (1989), Flow Resistance over A Gravel Bed; Its Consequence on Initial Sediment Movement, Key-note paper, Proc., International Workshop on Fluvial Hydraulics of Mountain Regions, Trent, Italy, pp.A1-A18.
7. Graf, W.H and M. Altinakar (1991), Hydrodynamique, Eyrolles, Paris.
8. Graf, W.H. and L.Suszka (1987), Sediment transport in Steep Channels, J.Hydroscience and Hydraulic Engineering, Jap. Soc. Civ. Engrs, Vol.5, No.1, pp.11-26.
9. Grishanin, K (1979), Dynamika Ruslobich Potokob (Dynamics of Alluvial Flow), Hydrometeoizat, Leningrad.
10. Kironoto, B. and W. H. Graf (1989), Decelerating Flow in A Gravel-Bed Flume, Rapport d'Activité, LRH-EPFL.
11. Li Z., Y. Chen and Y. Zhao (1983), Laboratory Investigation on Drag and Lift Forces Acting on Bed Spheres, Proceedings of the 2nd International Symposium on River Sedimentation, Nanjing, China, pp.330-343.
12. Nakagawa, H., T. Tsujimoto (1983), Time Lag Appearing in Unsteady Flow with Sand Waves, J.Hydroscience and Hydraulic Engineering, Jap. Soc. Civ. Engrs, Vol.1, No.1, pp.83-95.
13. Nezu, I and W. Rodi (1986), Open Channel Flow Measurements with a Laser Doppler Anemometer, Proc., Am. Soc. Civ. Engrs, J.Hydraulic Engineering, Vol.112, No.HY5, pp.335-355.
14. Nouh, M. (1989), Self Armoring Process under Unsteady Flow Conditions, Proc. 23th IAHR Congress, Ottawa, Canada, pp.B49-B56.
15. Phillips, B. C. and A. J. Sutherland (1984), Spatial and Temporal Lag Effects in Bedload Transport, Report 84/10, Dept. Civil Engineering, Univ. Canterbury, New Zealand.
16. Suszka, L. (1987), Sediment Transport at Steady and Unsteady Flow; A Laboratory Study, Doctoral dissertation No.704, Laboratoire de Recherches Hydrauliques, Ecole Polytechnique Fédérale, Lausanne, Switzerland.
17. Tsujimoto, T. (1988), Bed-Load Transport in Unsteady Flow, Proc. 6th APD-IAHR Congress, Kyoto, Japan, Vol.II-2, pp.15-22.
18. Tu H., T.Tsujimoto and W.H.Graf (1988), Velocity Distribution in A Gravel-Bed Flume, Proc. 6th APD-IAHR Congress, Kyoto, Japan, Vol.II-2, pp.425-431.
19. Tu H. (1991), Velocity Distribution in Unsteady Flow over Gravel Beds, Doctoral dissertation No.911, Laboratoire de Recherches Hydrauliques, Ecole Polytechnique Fédérale, Lausanne, Switzerland.
20. Tu H. and W. H. Graf (1992), Friction in Unsteady Open-Channel Flow over Gravel Beds, accepted for publication in the J. Hydr. Res..
21. Tubino, M. (1989), Flume Experiments on Alternate-Bars in Unsteady Flow, Proc. International Workshop on Fluvial Hydraulics of Mountain Regions, Trent, Italy, pp.A93-A107.
22. White, F.M. (1974), Viscous Fluid Flow, McGraw-Hill, Inc., New York, p.725.

APPENDIX-NOTATION

The following symbols are used in this paper:

Br	= a numerical constant of integration in the log-law;
C	= wave velocity, $C = V + D\,\frac{\partial V}{\partial t}/\frac{\partial D}{\partial t}$;
D	= water depth;
D'	= the water height where the maximum point velocity in a velocity profile, u_{max}, is measured;
d_S	= median gravel diameter, $d_S = d_{50}$;
g	= gravitational acceleration;
Q	= flow discharge;
S_0	= bottom slope;
t	= time variable;
u	= longitudinal component of the point velocity;
u_{max}	= maximum velocity in a velocity profile;
u_{*sv}	= friction velocity calculated from the St. Venant equation;
V	= vertically-averaged velocity, $V = \frac{1}{D}\int_{y\to 0}^{D} u\ dy$;
x	= the longitudinal coordi-nate;
y	= vertical coordinate;
y_o	= reference-level adjustment;

$(y/D)_{av}$ = the relative water depth where the point velocity equals the vertically-averaged velocity, V;

β = Clauser parameter; $\beta = \frac{m^3}{[\kappa(1+m)(\frac{d_s}{D})^{1/m}]^2}(-\frac{D}{V^2}\frac{dV}{dx})$;

ΔT = total time duration of a hydrograph;

ΔT_r = time duration of the rising branch in a hydrograph;

ΔT_f = time duration of the falling branch in a hydrograph;

δ^* = displacement thickness;

κ = Karman constant;

m = viscosity coefficient;

Π = wake-strength parameter; and

ρ = fluid density.

(Received October 29, 1991; revised January 23, 1992)